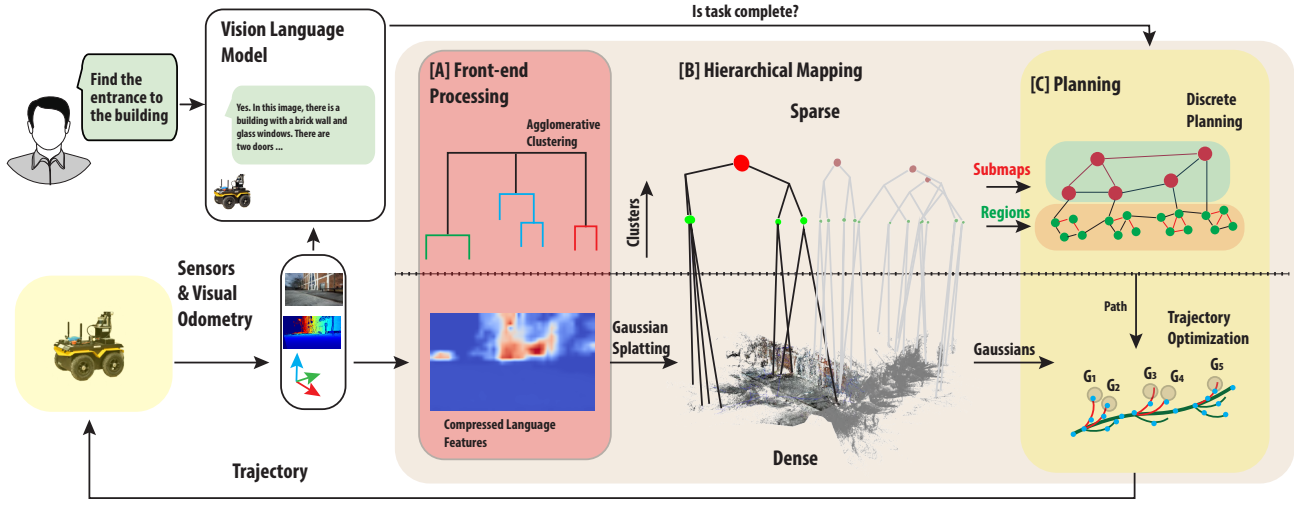


# ATLAS Navigator: Active Task-driven LAnguage-embedded Gaussian Splatting

Dexter Ong, Yuezhan Tao, Varun Murali, Igor Spasojevic, Vijay Kumar, Pratik Chaudhari

GRASP Laboratory, University of Pennsylvania

Email: {odexter, yztao, mvarun, igorspas, kumar, pratikac}@seas.upenn.edu



**Fig. 1:** Our framework consists of three components. The front-end processing [A] extracts and compresses dense pixel-level language features from the image. The module also clusters features based on geometry and semantics in the map. The hierarchical mapper [B] runs bottom-up, ingesting the RGB and depth images and the odometric path from the robot to build a map. The top level of the map contains the submaps, the middle level the regions, and the bottom level the objects. The local map compses the loaded submaps. The other submaps are unloaded to save memory (shown here in gray). The planning module [C] consists of a discrete planner that operates on the sparse map and generates a reference path, while the dense Gaussians in the local map are used to find the trajectory to be executed on the robot.

**Abstract**—We address the challenge of task-oriented navigation in unstructured and unknown environments, where robots must incrementally build and reason on rich, metric-semantic maps in real time. Since tasks may require clarification or re-specification, it is necessary for the information in the map to be rich enough to enable generalization across a wide range of tasks. To effectively execute tasks specified in natural language, we propose a hierarchical representation built on language-embedded Gaussian splatting that enables both sparse semantic planning that lends itself to online operation and dense geometric representation for collision-free navigation. We validate the effectiveness of our method through real-world robot experiments conducted in both cluttered indoor and kilometer-scale outdoor environments, with a competitive ratio of about 60% against privileged baselines. Experiment videos and more details can be found on our project page: <https://atlasnav.github.io>

## I. INTRODUCTION

The increasing deployment of robots in real-world environments for infrastructure inspection [1], search-and-rescue [2, 3] and agriculture [4] necessitates the development of systems capable of natural language interaction with humans, providing both textual and visual feedback. This, in turn, requires robots

to autonomously perceive their surroundings, gather relevant information, and make safe and efficient decisions – capabilities crucial for a variety of *open-world tasking approaches over kilometer-scale environments with sparse semantics*. To enable these capabilities on-board robots with privacy & compute constraints, we develop a framework to efficiently store and plan on hierarchical metric-semantic maps with visual and inertial sensors only. An overview of our method is shown in Fig. 1.

A cornerstone of autonomous navigation is the creation of actionable maps that effectively represent the environment and support diverse navigation and task-specific operations. Such maps must possess several key desiderata: (1) a consistent association between semantic and geometric information derived from observations, enabling a holistic understanding of the environment; (2) an efficient storage mechanism for navigation, such as a hierarchical organization of semantic information into submaps coupled with the representation of geometric information using Gaussian distributions, providing scalability and precise spatial modeling; and (3) task-relevant

identification and adaptability, achieved through scoring Gaussian components to facilitate generalization across various tasks and adaptation to new objectives.

These properties collectively ensure that the proposed map is not only manageable but also capable of supporting large-scale autonomous navigation to complete tasks provided in natural language. To achieve these goals, we propose an agglomerative data structure that is consistent across both geometric and semantic scales built upon 3D Gaussian Splatting [5] (3DGS). We extract semantics using a backbone vision-language model [6] and store a compressed feature vector alongside the gaussian points (see Sec. IV-A). This data structure integrates semantic and geometric information seamlessly, allowing for efficient navigation, and task-driven retrieval. The design addresses the key challenges of map storage, scalability, and task adaptability, making it suitable for real-world applications. A critical consideration in autonomous navigation is the ability to efficiently access and process relevant map information for motion planning. Therefore, the proposed map structure is designed to enable rapid, in-silico retrieval of the map region immediately surrounding the robot (required for efficient planning, see Sec. IV-B), allowing for timely and efficient local path planning. Simultaneously, the map must retain and manage long-range environmental information (see Sec. IV-A), providing a comprehensive understanding of the overall environment for tasks such as global path planning and loop closure.

Beyond these map storage requirements, we recognize the need for this actionable map to complement typical hierarchical motion-planning strategies, which often employ a discrete planner for high-level guidance and a low-level planner for dynamically-feasible and safe navigation. This allows for a **unified framework for mapping and planning from the same set of sensors** which allows our method to be deployed on low SWaP (size, weight & power) robots. In addition to the reduced computational and power burden of operation, this formulation allows us to mitigate any discrepancies in the maps used between mapping and planning. We formulate the planning problem within this two-stage framework (see Sec. IV-B) and leverage task-relevant scoring for utility calculation in the discrete planning problem, coupled with a sampling-based motion planner for dynamically-feasible trajectory generation.

The key contributions of this work are summarized as follows:

- **Memory-efficient online language-embedded Gaussian splatting:** We introduce a method for Gaussian splatting that incorporates language embeddings efficiently to optimize memory usage. This approach combines dimensionality reduction techniques, such as principal component analysis (PCA), with efficient online updates, ensuring that the map maintains a compact and scalable representation while preserving the necessary geometric and semantic fidelity.
- **Submapping with sparse semantic hierarchical clusters and dense geometry:** The proposed map is structured into sparse semantic clusters that represent regions

or objects and dense geometric representations for navigation. This design leverages a tectonic structure, which updates submap anchor poses after loop closure. As a result, the map is compatible with external odometry sources and pre-built maps, enabling consistent updates and large-scale navigation.

- **Large-scale ( $>km$ ) autonomous task-driven navigation with reusable maps:** Our approach supports task-driven navigation by dynamically identifying and retrieving map regions relevant to specific objectives. The system is also compatible with real-time, interactive task re-specification, allowing for adaptive exploration and navigation in large-scale environments.

We demonstrate these contributions through experiments that show the efficiency and semantic retrieval capability of our mapping framework on datasets (Sec. V-A), and real-world demonstrations of the full framework on a mobile robot (Sec. V-B).

## II. RELATED WORK

Our proposed work lies at the intersection of active perception, efficient language-embedded Gaussian splatting, hierarchical semantic-metric mapping and planning, and task-driven navigation. We propose a compact hierarchical language-embedded map representation built upon Gaussian splatting that can enable task-driven autonomous navigation while incrementally exploring and building a map of the environment.

### A. Active Perception

Active perception methods allow the robot to actively select actions and viewpoints that maximize the information gain relevant to a given task. This problem has been widely studied in volumetric representations such as voxel maps or Signed Distance Field (SDF) maps. In [7, 8, 9, 10], the information gain is evaluated as the mutual information between the current map and expected map given future observations. To accelerate the computation, information gain can be approximated with cell counting-based methods [11, 12, 13, 14, 15, 16, 17]. The information-driven approach has also been widely adopted for autonomous exploration with learned representations such as Neural Radiance Fields (NeRFs) or neural SDFs. Several approaches [18] estimate information gain in NeRFs by selecting future observations from a training dataset or by sampling viewpoints in the radiance fields [19, 20, 21, 22, 23]. In neural SDFs, [24] evaluates information gain as the variance of the model induced by parameter perturbations. The approach in [25] quantifies information gain by learning the reconstruction uncertainty with an MLP. Fisher Information has been used as the proxy for evaluating mutual information for 3D Gaussian splatting [26]. Combining a voxel map with 3D Gaussian Splatting, in [27], the information gain is evaluated as the weighted sum of unobserved volume between rays in the occupancy map, where the weights are determined by the transmittance of the Gaussians. The method has been further extended in [28], by incorporating Fisher Information as part of the information gain of a candidate viewpoint. Motivated by

the theory of Kalman filtering, [29] approximates uncertainty with the magnitude of the parameter updates of the map, which is then used for estimating the information gain of candidate viewpoints.

### B. 3D Gaussian Splatting

3D Gaussian splatting proposed in [5] provides a unique representation that captures geometry with Gaussians while encoding color and opacity information for high-quality rendering of scenes. Building upon this representation, several approaches focus on real-time construction of such maps with color and depth measurements in simultaneous localization and mapping (SLAM) frameworks. The method in [30] employs a silhouette mask on rendering for efficient optimization of the scene. The work in [31] addresses the monocular SLAM problem with 3DGS along with an analytical Jacobians for pose optimization. The authors of [32] propose handling Gaussian parameters differently for color and depth rendering by more explicitly representing surfaces for depth rendering, resulting in a more memory-efficient representation of the scene. Similarly, [33] estimates stability and uncertainty of the Gaussians for efficient representation of the scene. An advantage of the explicit representation of the Gaussian points is the ease of collision checking. In comparison with other works, most notably [34], we handle collision avoidance as chance constraints - in our case the size of the confidence ellipsoids depends on the number of Gaussians in the environment. There are also numerous methods that address the problem of scene understanding with language-embedded 3DGS. These approaches typically obtain 2D language features from Contrastive Language–Image Pre-training [35] (CLIP) and other foundation models, and distill these image features into 3D Gaussians. Methods in [36, 37, 38] use scene-specific autoencoders or quantization to obtain compact representations of the language features. Other approaches [39, 40] leverage feature fields similar to the method proposed in [41] for Neural Radiance Fields (NeRFs). In this work, we focus on an explicit representation that is amenable to planning. We associate every Gaussian point in the map with a language embedding that is subsequently compressed using its principal components, yielding a scene-agnostic language-embedded map.

A sub-class of approaches [42, 43] processes the scene as submaps by only optimizing the Gaussians on the submap level. The approach in [42] performs submap alignment using multi-view pose refinement on keyframes images. Similar to these methods, we use a submapping approach for efficient storage of the map, focusing instead on the problem of optimizing Gaussians across multiple submaps to facilitate large-scale navigation.

### C. Semantic Mapping and Task-based Navigation

Metric-semantic maps, which integrate both geometric and semantic information, provide actionable and informative representations of the environment. Common forms of metric-semantic maps include semantics-augmented occupancy maps [9, 44], object-based semantic maps [45] and

3D scene graphs [46, 47, 48, 49]. Among these, 3D scene graphs have emerged as a powerful representation, capable of capturing broader semantic concepts and the underlying contextual relationships within environments [46]. These models provide a compact, symbolic representation of semantic entities in the environments and their relationships [47, 48]. The concept of hierarchical representations of semantics and geometry was established by [46], which integrated multiple layers of information at increasing levels of abstraction. Others [49] incorporated additional information such as free space, object detections, and room categories on top of geometric representations. This was extended by [50] to incorporate structural elements (*e.g.* walls) and clustering rooms. Large Language Models (LLMs) have also been utilized to infer semantic relationships in the hierarchy [51] where structure is not readily available. To further generalize the use of scene graphs and capture a broader range of concepts for more complex robotic tasks, language features have been integrated to enable *open-set* scene understanding. Clio [52] constructs a hierarchical scene graph, where the set of objects and regions are inferred from the list of given tasks. Similarly, OrionNav [53] leverages open-set segmentation and LLM-based room clustering to build open-vocabulary scene graphs. ConceptGraphs [54] constructs open-vocabulary 3D scene graphs from RGB-D image sequences by leveraging 2D foundation models for instance segmentation and projecting semantic features into 3D point clouds. It fuses multi-view information to create 3D objects annotated with vision and language descriptors, and uses large vision-language models to generate object captions and infer inter-object relations, resulting in comprehensive 3D scene graphs. HOV-SG (Hierarchical Open-Vocabulary 3D Scene Graph) [55] extends these capabilities to large-scale, multi-story environments. It introduces a hierarchical structure encompassing floors, rooms, and objects, each enriched with open-vocabulary features derived from pre-trained vision-language models. While these methods that obtain an explicit semantic label at each level of a sparse, hierarchical representation capture the structure of known indoor environments, such approaches cannot be directly applied to unknown and unstructured environments. We instead try to find a balance between the sparsity provided by the hierarchical representation in scene graphs and the flexibility provided by dense, continuous feature embeddings.

### D. Task and motion planning

A fundamental challenge in task-driven planning (beyond mapping and exploration) is the identification of objects and following paths likely to result in localizing the object in the minimum possible time. [56] proposed a planner that prioritizes the discovery of objects of interest and ensures their complete and high-resolution reconstruction. Learning based approaches that estimate semantic maps beyond line of sight have also been proposed [57] utilizing confidence in semantic labels from unobserved regions to guide the search. Recent work has also focused on leveraging hierarchical scene graphs for semantic search tasks [58] using LLMs to guide

an optimal hierarchical planner for semantic search, although these approaches assume that the map is available *a priori*. Partially Observable Markov Decision Processes (POMDPs) have also been considered for planning on partially unknown scene graphs [59]. Reinforcement Learning based methods [60] have also been used to leverage scene graphs and graph neural networks to compute navigation policies, biasing the search toward regions of interest. Recently, Vision Language Frontier Maps (VLFM) [61] utilized a Vision-Language Model (VLM) for estimating the similarity between the task and images projected onto a bird's eye view to score frontiers by their relevancy. Large Language Models have also been directly used to select robot behaviors from a fixed library to select actions that minimize the time required to complete a task [62]. While these methods either focus entirely on completing the task with minimal maps along the way, we instead focus on generating a rich map that is reusable across a variety of tasks.

### III. PROBLEM FORMULATION

We consider the problem of optimizing the policy to minimize the time  $T$  it takes a robot to complete a given task. The robot dynamics are given by

$$x_{t+1} = f(x_t, u_t) + w_t, \quad (1)$$

where  $x_t \in \mathcal{X}$  and  $u_t \in \mathcal{U}$  are the state and control input of the robot at time  $t$ ,  $w_t$  is dynamics noise distributed according to  $\mathcal{N}(0, \Sigma_{dyn})$ , and the function  $f : \mathcal{X} \times \mathcal{U} \rightarrow \mathcal{X}$  represents the disturbance-free equation of motion. The state space  $\mathcal{X}$  is a subset of  $\mathbb{R}^{d_x}$  and the feasible control set  $\mathcal{U}$  is a bounded region in  $\mathbb{R}^{d_u}$ .

The true, initially unknown, map of the environment  $m^*$  belongs to the space of maps  $\mathcal{M}$ . In this work,  $\mathcal{M}$  is a vector of 3D Gaussian point parameters. The measurement received from the camera on board the robot at time  $t$  is given by

$$y_t = h(x_t, m^*) + v_t, \quad (2)$$

where  $h : \mathcal{X} \times \mathcal{M} \rightarrow \mathcal{Y}$  is the observation function,  $\mathcal{Y}$  is the vector space of images captured by the camera, and  $v_t$  is sensing noise distributed according to  $\mathcal{N}(0, \Sigma_{obs})$ . We assume that  $(v_t)_{t \geq 1}$  and  $(w_t)_{t \geq 1}$  are independent random variables. A policy is a sequence of functions  $\pi = (\pi_1, \pi_2, \dots)$  such that for each  $t \geq 1$ ,  $\pi_t$  is a function mapping the history of observations received up to time  $t$  to a control input  $u$ :

$$\pi_t : \underbrace{\mathcal{Y} \times \dots \times \mathcal{Y}}_{=: \mathcal{Y}^t} \rightarrow \mathcal{U} \quad \text{with} \quad u_t := \pi_t(y_{1:t}). \quad (3)$$

We assume that we are provided with an oracle function  $\Psi$  that determines whether the task has been completed or not. Each task is encoded by a feature vector  $z$  that belongs to the space of all tasks  $\mathcal{Z}$ , which lies in the same space as the natural language embedding vector. Since a task can be completed after a different number of observations, we define the set of all finite sequences of observations as  $\mathcal{Y}^* = \bigcup_{n \in \mathbb{N}} \mathcal{Y}^n$ . In this way, the oracle takes as input the task embedding and the

sequence of observations, and outputs the confidence regarding whether the task has been completed or not:

$$\Psi : \mathcal{Z} \times \mathcal{Y}^* \rightarrow [0, 1]. \quad (4)$$

Ultimately, we are interested in solving the following problem:

$$\begin{aligned} & \min_{\pi, T} \mathbb{E}[T] \\ & \text{subject to} \\ & \quad \Psi(z, y_{0:T}) = 1, \\ & \quad \text{and } \forall 1 \leq t \leq T : \\ & \quad x_{t+1} = f(x_t, u_t) + w_t \\ & \quad y_t = h(x_t, m^*) + v_t \\ & \quad \mathbb{P}(x_t \in \mathcal{X}_{free}) \geq 1 - \eta. \end{aligned} \quad (5)$$

The last constraint requires the robot to remain within the set of collision-free states  $\mathcal{X}_{free} \subseteq \mathcal{X}$  above a certain probability. In this way  $\eta \in (0, 1)$  represents the tolerance on the collision probability at each point in time. The expectation is taken over the randomness generated by the dynamics and sensing noise.

### IV. METHOD

We address the problem of task-based navigation and mapping while incrementally building a map of the environment that (1) provides a sparse, hierarchical and semantic representation for navigation that can be adapted for different tasks in real-time and (2) contains a dense geometric representation for collision-free planning. We first present the bottom-up hierarchical mapping approach and then the top-down planning approach. The methods interact with each other through new images acquired by taking an action.

We seek a solution to the problem within a subclass of policies. These policies first map the history of observations to a representation of the map as a vector of Gaussian parameters. They subsequently solve a trajectory planning problem that maximizes the progress towards achieving the specified task while retaining safety. Such a policy might be summarized in the following steps:

- 1)  $\hat{M}_t, \hat{x}_t \leftarrow MAPPER(y_{1:t})$  (described in section IV-A)
- 2)  $\mathcal{P}_{info} \leftarrow DISC(\hat{M}_t, \hat{x}_t)$  (described in section IV-B)
- 3)  $\mathcal{P}_{dyn} \leftarrow CTS(\hat{M}_t, \hat{x}_t, \mathcal{P}_{info})$  (described in section IV-B),

where  $DISC$  refers to the discrete planner and  $CTS$  refers to the continuous planner.

#### A. Hierarchical Semantic Perception

**Gaussian splatting.** A map of the scene is built with a set of Gaussians, each containing parameters comprising the mean  $\mu$ , covariance  $\Sigma$ , color  $c$  and opacity  $o$ . To render an image at a given camera pose, the Gaussians are sorted and splatted on to the image space. Each splatted 3D Gaussian will have a corresponding 2D mean  $\mu_{2D}$  and covariance  $\Sigma_{2D}$  in the image space. The color of a pixel  $p$  is obtained according to:

$$C_p = \sum_i^n c_i \alpha(p)_i \prod_{j=1}^{i-1} (1 - \alpha_j)$$

where

$$\alpha_i(p) = o_i \cdot \exp\left(-\frac{1}{2}(p - \mu_{2D,i})^T \Sigma_{2D,i}^{-1}(p - \mu_{2D,i})\right).$$

Depth can be similarly obtained by splatting the means of the Gaussians. In an incremental mapping approach, Gaussians are initialized at each mapping step and subsequently optimized. From a single color and depth observation, each pixel is back-projected to form a 3D pointcloud. A Gaussian is initialized at each 3D point with its corresponding color. The parameters of the Gaussians are optimized by rendering color and depth image through the differentiable rasterization process and a loss is computed against the original color and depth observations.

**Dense language features.** For each observation  $y_t$ , we extract dense pixel-level language features  $\mathbf{F}_t \in \mathbb{R}^{N_f}$  via the feature map  $\Phi : \mathcal{Y} \rightarrow \mathcal{Z}$ . In contrast to other approaches that compute and fuse multi-scale embeddings from CLIP and other foundation models, we use a lightweight approach from CLIP-DINOiser [6], which refines MaskCLIP [63] features by incorporating localization priors extracted with self-supervised features from DINOv2 [64].

**Language-embedded 3D Gaussian splatting.** We build our semantic mapping approach on language-embedded 3D Gaussian splatting. We optimize isotropic Gaussian parameters to enable rendering of scenes. In addition to color and opacity, we embed a compressed language feature vector  $\tilde{\mathbf{F}}_t \in \mathbb{R}^{N_c}$  in each Gaussian's parameters. For a given camera pose, a reconstructed feature image  $\hat{\mathbf{F}}_t \in \mathbb{R}^{N_c}$  is rendered from the scene and the loss is computed against the original compressed feature image  $\tilde{\mathbf{F}}_t$  to optimize the Gaussian parameters.

**Feature compression.** To capture rich semantic information, language features are typically high-dimensional vectors. For efficient computation and storage of language features in the Gaussians' parameters, we require a compact representation of the language features in the form of  $\tilde{\mathbf{F}}$ .

Most language-embedded Gaussian splatting approaches leverage alternate representations like features fields [41, 39] or scene-specific autoencoders [37] to obtain  $\tilde{\mathbf{F}}$ . However, these approaches do not generalize well to new and unknown environments. We perform dimensionality reduction on the feature space via Principal Component Analysis (PCA). To obtain a representative distribution of CLIP embeddings, we use Incremental Principal Component Analysis [65] (IPCA) to fit the COCO [66] 2017 dataset. We note that different and larger datasets can be used as well. The computation of the basis vectors is done offline. At runtime, we simply need to project the features on to these vectors to obtain the principal components.

For each image, we extract the full  $N_f$ -dimensional language features, obtain the first  $N_c$  principal components and embed them in the map through the 3D Gaussian splatting process. We can then recover the original dimensions of the features with the inverse of the PCA for computing similarity with the task embeddings.

**Submapping.** In this work, we augment the 3D Gaussian splatting framework with submaps. As the robot navigates

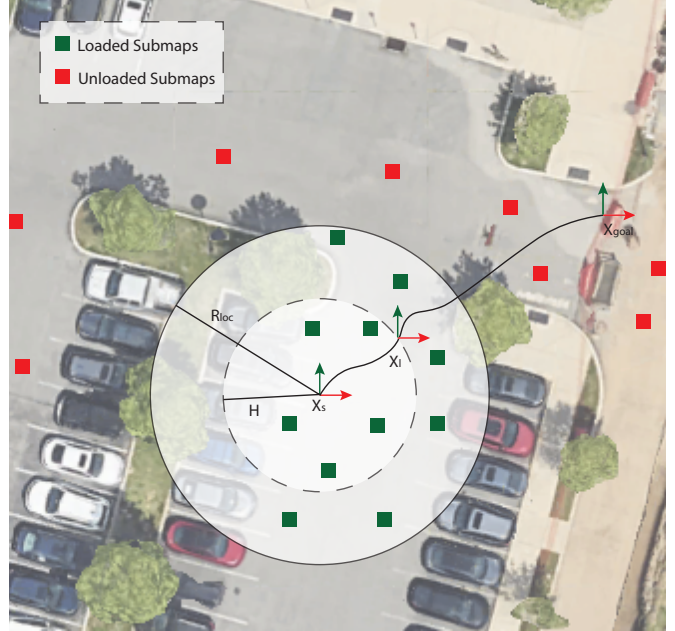


**Fig. 2:** An illustration of the different parameters that are relevant to the submapping and collision checking process.  $X_s$  denotes the current position of the robot,  $X_l$  is the local goal along the path to the final goal  $X_{goal}$ . Submaps are loaded within the region bounded by  $R_{loc}$ .

the environment, it receives color and depth measurements together with its estimated odometry, and incrementally builds a map. Since Gaussians are added at every mapping iteration, the number of Gaussians in the map can quickly grow to the order of millions of Gaussians and this can be challenging to manage on a SWaP-constrained robot. To enable large-scale operations, our proposed mapping system efficiently creates submaps as the robot explores the environment.

By design, each submap contains a 6 degree-of-freedom (DoF) anchor pose which serves as the reference frame of its local coordinate system. The submap stores all parameters of the 3D Gaussians relative to the anchor pose. In every mapping iteration, the robot loads all submaps within the range  $R_{loc}$  into the GPU memory and offloads any other submaps that are currently on the GPU. If there are no submaps within a specified range  $r_{submap}$ , the robot creates a new submap with a unique ID and the last odometry measurement as the anchor pose. Every Gaussian instantiated from a measurement  $y_t$  is associated with the submap corresponding to  $x_t$ . These Gaussians are stored in the local reference frame of the submap.

The submap design ensures safe and efficient navigation while significantly reducing the number of Gaussians that need to be considered by the continuous planning module IV-B. As an example, in Fig. 2, the continuous planning module only plans on a map with 369,513 Gaussians instead of the global map which contains 2.47 million Gaussians. This drastically reduces the number of operations for collision checking and hence improves the planning efficiency. In contrast to traditional

tional voxel-based mapping that has a fixed discretization, our map design does not preallocate memory for the Gaussians, allowing for a flexible storage structure. This flexibility allows for denser maps in cluttered environments and sparser maps in large open spaces.

Our submap design can also accomodate pose corrections from any underlying Simultaneous Localization and Mapping (SLAM) algorithm. This ensures map consistency across large-scale operations with multiple loop closures. Our method incorporates external pose graph corrections by updating the anchor poses of the submaps. For efficiency, we assume that the keyframes associated with each submap are locally consistent and are rigidly attached to the submap reference frame.

**Metric-semantic clustering** In unstructured environments, approaches such as those in [54, 52, 55] that use image segmentation priors may fail to give meaningful object clusters. We instead perform metric-semantic clustering on the language-embedded Gaussians directly. For the set of Gaussians in each submap, we compute the pairwise distances  $q$  between all points using a sum of Euclidean distance  $q_e$  and cosine-similarity  $q_s$  of the compressed language feature vectors of each Gaussian, weighted by a parameter  $\lambda$ .

$$q = q_e + \lambda \cdot (1 - q_s)$$

With the computed distance matrix, we perform agglomerative clustering to create object-level clusters in a hierarchy. For this work, we partition these clusters into three levels – the submap, region and object levels. We note that unlike other feature compression methods, we can perform this clustering with our embedded features directly since the components from IPCA still retain important semantic features. This negates the need to recover the full feature dimensions, allowing for efficient dense clustering online.

For a given task, we compute the utility of each submap by querying the object-level clusters to obtain a task-relevancy score. These clusters would correspond to the leaf nodes of the tree. From these clusters, we propagate the object-level relevancy up the tree to obtain utility scores for region- and submap-level nodes. Following Eq. 8, the utility of each node in the tree is the sum of the utilities of its children. The utility at the root of the tree serves as the corresponding utility of that submap. This submap-level cluster information is stored in each submap along with the Gaussian splatting parameters.

### B. Hierarchical Planning

Since we care about potentially large-scale environments, we turn our attention to a hierarchical planning strategy with a discrete planner responsible for long-term reasoning and a continuous trajectory planner responsible for finding dynamically-feasible trajectories.

**Problem 1: Discrete planning.** Given a set of vantage points and their associated utilities  $(X, \Gamma)$  and task embedding  $z$ , we find the optimal sequence of vantage points  $\mathcal{P} = x_1 x_2 \dots x_k$  that maximizes the utility along the path while staying within a given travel budget  $\mathcal{B}$ .

Letting  $w$  be a function on pairs of points  $w : (x_i, x_j) \rightarrow [0, \infty)$ , we solve

$$\begin{aligned} & \max_{\mathcal{P}=(x_{1:k})} \psi(z, y_{0:k}) \\ & \text{subject to} \\ & \sum_{i=1}^{k-1} w(x_i, x_{i+1}) \leq \mathcal{B} \\ & y_k = h(x_k, m) \quad \forall x_k \in \mathcal{P} \end{aligned} \tag{6}$$

Problem 1 requires us to find a sequence of vantage points (through the sparse components of the map in Fig. 1) from which the collected images  $y_{0:k}$  maximize the chance of completing the task. We make a few simplifying assumptions at this stage: (i) that the locations are not correlated *i.e.* that taking a measurement at  $x_i$  does not affect the utility of  $x_j \forall j \neq i$ ; (ii) the path between a pair of points with weight  $w \leq d_{\text{wire}}$  lies in free-space and (iii) visiting a vertex is enough to collect the information regardless of the orientation required for acquiring the image from the vantage point.

With these assumptions, we can construct this problem as a graph search problem. We construct a graph  $G = (V, E)$ , whose vertices are the set of vantage points  $X$ . The utility function  $\Gamma : V \rightarrow [0, \infty)$  specifies the utility of each vertex. The weight function on the edges is then  $w : E \rightarrow [0, \infty)$  which is the Euclidean distance between the vertices. To find the optimal path we seek to solve the following problem:

$$\begin{aligned} & \max_{\mathcal{P}=(x_{1:k})} \sum_{i=1}^k \Gamma(x_i) \\ & \text{subject to} \\ & \sum_{i=1}^{k-1} w(x_i, x_{i+1}) \leq \mathcal{B} \end{aligned} \tag{7}$$

Since the number of possible vertices is large & we desire an efficient solution on-board low SWaP robots, we solve the latter problem in a hierarchical fashion. We assume the set of vertices is partitioned according to  $V = \cup_{i=1}^p V_i$  where  $V_i \cap V_j = \emptyset$  for all  $i \neq j$ . We form a high level graph  $\tilde{G} = (\tilde{V}, \tilde{E})$  whose vertex set  $\tilde{V} = \{\tilde{v}_1, \tilde{v}_2, \dots, \tilde{v}_p\}$  corresponds to centroids of vertices in each partition. For each vertex  $\tilde{v}_i$  in  $\tilde{V}$ , we add an edge between  $\tilde{v}_i$  and  $\tilde{v}_j$  if  $\|\tilde{v}_i - \tilde{v}_j\|_2 \leq d_{\text{wire}}$  for a user-defined parameter  $d_{\text{wire}}$ . Our path planning problem then involves finding the optimal path through this weighted graph whose cost does not exceed a given budget. The set of edges  $\tilde{E} \subseteq \tilde{V} \times \tilde{V}$ . The weight function  $\tilde{w} : \tilde{E} \rightarrow [0, \infty)$  specifies the weight of every edge in  $\tilde{G}$  as the distance between centroids corresponding to the endpoint vertices. The utility of every vertex in  $\tilde{G}$  is given by the function  $\tilde{\Gamma} : \tilde{V} \rightarrow [0, \infty)$ , with

$$\tilde{\Gamma}(\tilde{v}_i) := \sum_{v \in V_i} \Gamma(v). \tag{8}$$

We first solve the high level problem:

$$\begin{aligned} & \max_{\tilde{\mathcal{P}}=(\tilde{x}_{1:k})} \sum_{i=1}^k \tilde{\Pi}(\tilde{x}_i) \\ & \text{subject to} \\ & \sum_{i=1}^{k-1} \tilde{w}(\tilde{x}_i, \tilde{x}_{i+1}) \leq \mathcal{B}. \end{aligned} \quad (9)$$

We then plan the path through  $G$  that visits the partitions  $V_i$  in the order specified by the sequence of edges in  $\mathcal{P}$ .

**Continuous trajectory planning.** For the purpose of synthesizing feasible trajectories, we model the robot as an agent with unicycle dynamics. Its state  $x = [p, \theta] \in \mathbb{R}^2 \times S^1$  consists of its position (on the ground plane  $z = 0$ ), and heading angle  $\theta$ . The control input  $u = [v, \omega] \in \mathbb{R}^2$  consists of the translational and angular speed of the robot. Its equations of motion are given by  $\dot{x} = f(x, u)$ , where  $f : \mathbb{R} \times S^1 \times \mathbb{R}^2 \rightarrow \mathbb{R}^2 \times \mathbb{R}$  is defined as

$$f(x, u) = \begin{bmatrix} \cos \theta & 0 \\ \sin \theta & 0 \\ 0 & 1 \end{bmatrix} \begin{bmatrix} v \\ \omega \end{bmatrix}. \quad (10)$$

The trajectory generation problem involves finding a dynamically feasible trajectory (per eq 11) that interpolates a given pair of boundary conditions. We solve the problem as part of a receding horizon control scheme. It is resolved at a set frequency, with the boundary conditions and free space updated using information based on accrued measurements. We choose the furthest point along the path provided by the Discrete Planner that is within our planning horizon  $H$  and treat this as the center of our goal region  $\mathcal{X}_{goal}$  for each iteration.

**Problem 2: Continuous Trajectory Planning.** Given an initial robot state  $x_0 \in \mathcal{X}_{free}$ , and goal region  $\mathcal{X}_{goal}$ , find the control inputs  $u(\cdot)$  defined on  $[0, \tau]$  that solve:

$$\begin{aligned} & \min_{u(\cdot), \tau} J(u(\cdot), \tau) \\ & \text{s.t. for all } t \in [0, \tau] \\ & \dot{x}(t) = f(x(t), u(t)), \quad x(t) \in \mathcal{X}_{free}, \\ & \|v(t)\|_2 \leq v_{max}, \quad |\omega(t)| \leq \omega_{max}, \\ & x(0), \theta(0) = x_0, \theta_0, \quad x(\tau) \in \mathcal{X}_{goal}. \end{aligned} \quad (11)$$

Problem 2 is a high-dimensional non-convex optimization problem. Two key hurdles from a computational standpoint are the nonlinear dynamics of the robot as well as the presence of obstacles in the environment. We therefore adopt a search-based procedure, motivated by the idea presented in [67]. In particular, we seek the minimum weight path in a directed graph formed by discretizing the continuous state space of the robot. The vertices of the graph correspond to select states, whereas the edges correspond to motion primitives emanating from a particular state that remain within  $\mathcal{X}_{free}$ . Each motion primitive is obtained by integrating a feasible fixed control input for a time interval  $\delta t$ . This ensures that any path through the graph represents a dynamically viable trajectory without

taking collisions into account. The set of fixed controls is represented as the Cartesian product of uniform discretizations of spaces of feasible translational and angular speeds. The set of feasible translational (angular) speeds,  $[-v_{max}, v_{max}]$  ( $[-\omega_{max}, \omega_{max}]$ ), is discretized by a grid of size  $N_v$  ( $N_\omega$ ). In order to determine whether an edge of the graph lies in free space, we first discuss how we check whether the robot collides with an object in the environment. To this end, we treat the robot as a normal random variable  $R \sim \mathcal{N}(\mu_{rob}, \Sigma_{rob})$  with mean  $\mu_{rob} \in \mathbb{R}^3$  and covariance  $\Sigma_{rob} \in S_{++}^3$ . We consider the robot to be in collision with a Gaussian point represented by the normal random variable  $G_i \sim \mathcal{N}(\mu_i, \Sigma_i)$  if their distance is below a specified collision radius  $r_{coll} > 0$ . Defining the predicate  $collide(R, G)$  that evaluates to true if the realizations of  $R$  and  $G$  represent a configuration in which a collision occurs, we have

$$collide(R, G_i) \Leftrightarrow \|R - G_i\|_2 \leq r_{coll}. \quad (12)$$

Since we have an uncertain map, the chance constraint  $\mathbb{P}(x \in \mathcal{X}_{free}) \geq 1 - \eta$  amounts to

$$\mathbb{P}(\bigcup_{G_i \in \hat{M}} collide(R, G_i)) \leq \eta, \quad (13)$$

where  $R$  is a random normal variable whose mean consists of the translational components of  $x$ , and whose variance is equal to  $\Sigma_{rob}$ . We consider an edge of the graph corresponding to a motion primitive to lie within  $\mathcal{X}_{free}$  just when each of the discretization points along the edge are collision-free per the equation above.

Since the number of Gaussians representing the environment is often very large, we compute approximate collision probabilities in a way that does not require iterating through all the Gaussians for every potential collision point. To prune away a large number of collision checks at the expense of a specified (small) tolerance in the error of estimation of the collision probability, we seek the smallest “local radius”  $R_{loc}$  such that the probability of colliding with obstacles whose means lie within the radius is to within  $p_{tol}$  of colliding with any of the obstacles in the whole environment. The main point is that a smaller value of  $R_{loc}$  allows us to focus on collision checking within a localized region of space, thus significantly decreasing both the running time and memory complexity of the collision-checking procedure without sacrificing safety of the robot. To determine a meaningful value of  $R_{loc}$ , we seek an upper bound on the probability of collision with a Gaussian point whose mean lies at distance at least  $R_{loc}$  from the robot. From the union bound, we have

$$\begin{aligned} & P(\exists G_i \in \hat{M} : \| \mu_i - \mu_{rob} \|_2 \geq R_{loc}, collide(R, G_i)) \leq \\ & \sum_{i : \| \mu_i - \mu_{rob} \|_2 \geq R_{loc}} P(collide(R, G_i)). \end{aligned} \quad (14)$$

Assuming that  $R$  and  $G_i$  are independent normal variables, we have that

$$R - G_i \sim \mathcal{N}(\mu_{rob} - \mu_i, \Sigma_{rob} + \Sigma_i), \quad (15)$$

resulting in

$$\begin{aligned} \mathbb{P}(\text{collide}(R, G_i)) &= \\ \mathbb{P}(\|(\mu_{rob} - \mu_i) + (\Sigma_{rob} + \Sigma_i)^{\frac{1}{2}} Z_{std}\|_2 \leq r_{coll}), \end{aligned} \quad (16)$$

where  $Z_{std} \sim \mathcal{N}(0, I_3)$  is a standard normal random variable used throughout the subsection. To make the calculation above more tractable, we assume that  $\Sigma_{rob} = \text{diag}(\sigma_{rob}^2, \sigma_{rob}^2, \sigma_{rob}^2)$  and  $\Sigma_i = \text{diag}(\sigma_i^2, \sigma_i^2, \sigma_i^2)$ . Hence we get

$$\begin{aligned} \mathbb{P}(\text{collide}(R, G_i)) &= \\ &= \mathbb{P}\left(\left\|\frac{\mu_{rob} - \mu_i}{\sqrt{\sigma_{rob}^2 + \sigma_i^2}} + Z_{std}\right\|_2 \leq \frac{r_{coll}}{\sqrt{\sigma_{rob}^2 + \sigma_i^2}}\right) \\ &= \mathbb{P}\left(Z_{std} \in \mathcal{B}\left(\mathbf{e}_1 \frac{\|\mu_{rob} - \mu_i\|_2}{\sqrt{\sigma_{rob}^2 + \sigma_i^2}}; \frac{r_{coll}}{\sqrt{\sigma_{rob}^2 + \sigma_i^2}}\right)\right), \end{aligned} \quad (17)$$

where the last inequality follows from the isotropic nature of the standard normal random variable. Plugging in the latter equality into the union bound, and denoting

$$S_{far}(R_{loc}) = \{G_i \in \hat{M} : \|\mu_i - \mu_{rob}\|_2 \geq R_{loc}\}, \quad (18)$$

we get

$$\begin{aligned} \mathbb{P}(\exists G_i \in \hat{M} : \|\mu_i - \mu_{rob}\|_2 \geq R_{loc}, \text{collide}(R, G_i)) &\leq \\ \sum_{S_{far}} P\left(Z_{std} \in \mathcal{B}\left(\mathbf{e}_1 \frac{\|\mu_{rob} - \mu_i\|_2}{\sqrt{\sigma_{rob}^2 + \sigma_i^2}}; \frac{r_{coll}}{\sqrt{\sigma_{rob}^2 + \sigma_i^2}}\right)\right) &\leq \\ \sum_{S_{far}} \mathbb{P}\left(Z_{std} \in \mathcal{B}\left(\mathbf{e}_1 \frac{R_{loc}}{\sqrt{\sigma_{rob}^2 + \sigma_i^2}}; \frac{r_{coll}}{\sqrt{\sigma_{rob}^2 + \sigma_i^2}}\right)\right) &\approx \\ |\{S_{far}(R_{loc})\}| \mathbb{P}\left(Z_{std} \in \frac{\mathcal{B}(\mathbf{e}_1 R_{loc}; r_{coll})}{\sqrt{\sigma_{rob}^2 + \sigma_{avg}^2}}\right), \end{aligned} \quad (19)$$

where in the last equality we made the approximation that the characteristic size of Gaussian points is  $\sigma_{avg}$ . Finally, we assume that the density of Gaussian points is approximately uniform, and equal to  $\rho$ . Therefore, denoting the number of all Gaussians in the global map by  $N$ , we make the last approximation

$$|\{G_i \in \hat{M} : \|\mu_i - \mu_{rob}\|_2 \geq R_{loc}\}| \approx \left(N - \frac{4}{3} R_{loc}^3 \pi \rho\right), \quad (20)$$

resulting in the following estimate

$$\begin{aligned} P(\exists G_i \in \hat{M} : \|\mu_i - \mu_{rob}\|_2 \geq R_{loc}, \text{collide}(R, G_i)) &\lesssim \\ \left(N - \frac{4}{3} R_{loc}^3 \pi \rho\right) P\left(\mathcal{N}(0, I_3) \in \frac{\mathcal{B}(\mathbf{e}_1 R_{loc}; r_{coll})}{\sqrt{\sigma_{rob}^2 + \sigma_{avg}^2}}\right). \end{aligned} \quad (21)$$

We are interested in finding the smallest  $R_{loc}$  so that the very last expression, a monotonically decreasing function of  $R_{loc}$ , is below a specified tolerance  $p_{tol}$ . Algorithmically we find this value via binary search (on the value of  $R_{loc}$ ).

The expression for the probability that a standard normal random variable in 3D lies inside the ball  $\mathcal{B}(\mathbf{e}_1 a; b)$  may be obtained as

$$\begin{aligned} \text{prob}(a, b) &= \\ &= \int_{a-b}^{a+b} \frac{dx}{\sqrt{2\pi}} e^{-\frac{x^2}{2}} \left(1 - \exp\left\{-\frac{1}{2}(b^2 - (x-a)^2)\right\}\right) \\ &= \int_{a-b}^{a+b} \frac{dx}{\sqrt{2\pi}} e^{-\frac{x^2}{2}} - \frac{\exp\left\{\frac{1}{2}(a^2 - b^2)\right\}}{\sqrt{2\pi}} \int_{a-b}^{a+b} e^{-ax} dx \\ &= F_{normal}(c) \Big|_{c=a-b}^{c=a+b} - \frac{\exp\left\{-\frac{1}{2}((a-b)^2 - (a+b)^2)\right\}}{\sqrt{2\pi} a}, \end{aligned} \quad (22)$$

where  $F_{normal}(c) := \int_{-\infty}^c \frac{dx}{\sqrt{2\pi}} \exp\left\{-\frac{x^2}{2}\right\}$  is the cumulative distribution function of the 1D standard normal variable. In the previous equation, we used the elementary fact that the probability that the standard normal variable in 2D lies outside a sphere (in this case - disk) of radius  $r$  centered on the origin is  $\exp\{-\frac{r^2}{2}\}$ . Furthermore, for a fixed value of  $b > 0$ ,  $\text{prob}(a, b)$  is a monotonically decreasing function of  $a$  on  $[0, \infty)$ . The latter observation may easily be seen by noting that the reflection about the plane that passes through the midpoint of two spheres ( $S_{near}$  and  $S_{far}$ ) of the same radius whose centers lie on a ray emanating from the origin, with the center of  $S_{near}$  being closer, maps  $S_{near} \setminus S_{far}$  to  $S_{far} \setminus S_{near}$  in a way that leaves the Lebesgue measure intact while decreasing the density of the standard normal variable.

The cost of each valid motion primitive is defined as

$$J(u(\cdot), \tau) := \lambda_t \tau + (v^2 + w^2) \tau,$$

where  $\lambda_t$  weights the time cost with the control efforts. Since the maximum velocity of the robot is bounded by  $v_{max}$ , we consider the minimum time heuristic as

$$h(p) := \|p_{goal} - p\|_2 / v_{max}.$$

Finally, we use A\* to search through the motion primitives tree.

### C. Implementation details

1) *Mapping*: We build our mapping module on the Gaussian splatting method presented by [30]. The most significant modifications are the submapping framework with pose estimates from visual-inertial odometry and the addition of Gaussian parameters for the language features. We note that any other Gaussian splatting method can be used as well if it can meet the compute and latency requirements. We compress the  $N_f = 512$  dimensional CLIP features to  $N_c = 24$  dimensions for embedding in the Gaussian parameters. We set the submap size  $r_{submap}$  to 2 meters for indoor experiments and 5 meters for outdoor experiments. We resize the image stream to  $320 \times 240$  for mapping and set the maximum depth range to 5 meters. To balance compute resources between the various modules, we limit the map update rate to 1 Hz.

2) *Planning*: We implemented both the discrete and continuous planning module in Python 3.8 with Pytorch 2.4.1 and implement the motion planning library from [67]. We set  $p_{tol}$  to 0.001 and  $\sigma_{rob}$  to 0.7 meters, and compute  $R_{loc}$  to be 10 meters. The planning horizon  $H$  is set to 5 meters. We adopted the idea of parallelized collision checks from [29] to enable efficient continuous planning online. The discrete planner runs onboard the robot every 5 mapping iterations while the continuous planner runs at 1 Hz.

3) *Task specification*: The task is specified in natural language by the user. We use a Vit-B-16 encoder for the CLIP backbone. Text embeddings are computed from the task prompt using the CLIP text encoder [38]. These text embeddings are used for computing the relevancy of the feature embeddings in the map to the task. Task re-specification is done in the same way. In addition, the relevancy of all submap object clusters are recomputed and their relevancy scores are propagated up the hierarchical tree of each submap. We note that we do not need to re-cluster the submaps for each new task and only need to recompute the relevancy of the features embeddings of the clusters. Hence we have a consistent hierarchical submap structure that can be efficiently re-queried for various tasks.

4) *Task termination*: We use LLaVA OneVision [68] to determine if the task has been completed. Given the language features of the current observation, we mask out pixels that are beyond the maximum depth range and compute the relevancy of the remaining pixels against the task. If the relevancy is beyond a threshold, we query the VLM module with the image and the task. We ask it to reply with a yes or no and a description of the scene. One such example is visualized in Fig. 7.

5) *Robot Platform*: In all of our robot experiments, we used a Clearpath Jackal robot platform. It is modified to carry an onboard computer with AMD Ryzen 5 3600 CPU, NVIDIA RTX 4000 Ada SFF GPU and 32 GB of RAM. Additionally, the robot is equipped with a ZED 2i stereo camera for obtaining RGB, depth and pose measurements using the first generation position tracking module. It also carries an Ouster OS1-64 LiDAR to generate ground truth odometry for evaluation.

## V. EXPERIMENTAL EVALUATION

We design our experimental protocol to first evaluate each component of our method with prior work for fair comparison and then demonstrate the full framework on a real robot. The key attributes of our mapping method are: (i) 3D Semantic Segmentation; (ii) Submapping; (iii) Memory Efficiency and (iv) Retrieval of objects in the pre-built maps. Further, we demonstrate closed-loop autonomy through real robot experiments, with and without a prior map.

### A. Dataset Experiments

1) *Open-vocabulary 3D semantic segmentation*: We evaluate the 3D semantic segmentation performance of our mapping approach on the ScanNet [69] dataset, using scenes:

scene0011\_00, scene0050\_00, scene0231\_00, scene0378\_00, scene0518\_00.

**Metrics.** We compute the mean Intersection Over Union (mIOU), mean accuracy (mAcc) and frequency-weighted mIOU (F-mIOU) following the same procedure in [55].

**Results.** The results are presented in Table I. ConceptGraphs [54] and HOV-SG [55] leverage image segmentation priors for creating object clusters and maintain sparse language feature vectors for each object. In contrast, ConceptFusion [70] is more similar to our work and stores dense language features in the map. We note that ConceptFusion also uses image segmentation priors for extracting local features on an object level. With our compressed language feature representation and without using image segmentation priors, we are able to achieve comparable performance with the baselines. We note that we also use a smaller CLIP backbone compared to the baseline methods.

Method	Feature embeddings	mIOU	mAcc	F-mIOU
ConceptGraphs [54]	Sparse	0.16	0.20	0.28
HOV-SG [55]		<b>0.22</b>	<b>0.30</b>	<b>0.43</b>
ConceptFusion [70]	Dense	0.11	0.12	0.21
ATLAS (ours)		0.15	0.27	0.16

**TABLE I:** Open-vocabulary 3D semantic segmentation on ScanNet. Baseline results from [55]. Baselines use Vit-H-14 while our method uses Vit-B-16 for the CLIP backbone.

2) *Loop closure*: To evaluate the effectiveness of pose correction with submaps, we generate maps from the same set of data. We generate three maps, one with just VIO pose estimates, one with the addition of PGO, and finally one with submap anchor pose updates on top of the PGO. We use LiDAR odometry [71] to obtain groundtruth poses for the test set. We compare the rendered images from each map and evaluate the rendering quality. Finally, to present the upper bound of the Gaussian splatting approach on this dataset, we also generate a map using the test set poses.

**Metrics.** We evaluate the Peak Signal-to-Noise Ratio (PSNR), Structural Similarity Index [72] (SSIM), Learned Perceptual Image Patch Similarity [73] (LPIPS) on the color images and Root Mean-Square-Error (RMSE) on the depth images.

**Results.** The results are presented in Table II. We show that we are able to leverage PGO with our submap-based mapping framework to achieve better reconstruction quality.

3) *Memory*: To highlight the value of the dynamic loading of submaps, we evaluate several 3DGS approaches on a large indoor scene. We use scene 00824 from the Habitat Matterport 3D Semantics Dataset [74] (HM3D), following the method in [55] to generate groundtruth observations and poses. If they support submapping, methods are evaluated with different submap sizes, at 2m and 5m distances between each submap. We note that Gaussian-SLAM and LoopSplat both employ submapping but only unload submaps and do not handle reloading and updating of submaps.

Method	PSNR $\uparrow$ (dB)	SSIM $\uparrow$	LPIPS $\downarrow$	RMSE $\downarrow$ (m)
VIO	12.62	0.53	0.48	0.89
VIO + PGO	14.09	0.54	0.47	0.85
VIO + PGO + SU	14.31	0.59	0.44	0.76
GT	<b>16.13</b>	<b>0.65</b>	<b>0.37</b>	<b>0.39</b>

**TABLE II:** Evaluation of loop closure-aware submap pose graph update. VIO refers to visual-inertia odometry, PGO refers to pose graph optimization, SU refers to submap anchor pose updates and GT refers to the ground truth poses. This experiment shows that our method is able to correct past poses by shifting the submap anchors.

**Results.** The results are presented in Table. III. Gaussian-SLAM [43] and LoopSplat [42] require large amounts of memory even at relatively small submap sizes. The results highlight that many Gaussian splatting SLAM methods cannot support memory-efficient mapping of large-scale environments, even on the scale of indoor environments. Ensuring efficient scaling of memory is crucial for operation on robots with limited compute.

Method	Memory Allocated / Reserved (GB)		
	2m submap	5m submap	No submap
Gaussian-SLAM [43]	<b>5.71</b> / 36.21	×	×
LoopSplat [42]	9.03 / 21.33	×	×
SplaTAM [30]	–	–	<b>13.36 / 16.32</b>
ATLAS (ours)	8.28 / <b>9.68</b>	<b>9.77 / 12.51</b>	<b>13.36 / 16.32</b>

**TABLE III:** Comparison of memory performance on scene 0011 of the HM3D dataset. – indicates that the method does not support submapping and is not evaluated with submaps.  $\times$  indicates that the method failed due to excessive memory requirements or otherwise. Gaussian-SLAM and LoopSplat are evaluated with submaps.

4) *Image rendering from built map:* Finally, a feature of our method is the ability to query images of relevance and provide textual feedback. We compare this functionality with HOV-SG [55] since they generate a dense colored point cloud. The resolution of the point cloud generated by HOV-SG is set to the default of 0.05m. Since HOV-SG stores dense features in each point, increasing the resolution of the point cloud is too expensive in terms of both compute and memory. We generate images from the point cloud by projecting the points using the corresponding camera intrinsics of the scene. We render images with both methods for all poses in the dataset. For this comparison, we use scene 0011 from the ScanNet [69] dataset. In addition to this, we show a qualitative result of the retrieval capability of our method from a pre-built map, constructed from data collected by tele-operating our robot.

**Metrics.** We evaluate the image reconstruction quality using the following metrics – Peak Signal-to-Noise Ratio (PSNR), Structural Similarity Index [72] (SSIM), Learned Perceptual Image Patch Similarity [73] (LPIPS) on the color images and Root Mean-Square-Error (RMSE) on the depth images.

**Results.** We evaluate the rendered images from each method using the original images of the ScanNet dataset as groundtruth. The results are presented in Table IV. While we

Method	PSNR $\uparrow$ (dB)	SSIM $\uparrow$	LPIPS $\downarrow$	RMSE $\downarrow$ (m)
HOV-SG [55]	6.86	0.22	0.90	1.95
ATLAS (ours)	<b>20.44</b>	<b>0.80</b>	<b>0.26</b>	<b>0.05</b>

**TABLE IV:** Image rendering quality on ScanNet.

acknowledge that the map representation used in HOV-SG does not prioritize rendering of the scene, we present these results to highlight the value of storing the map as Gaussian parameters. The qualitative evaluation of the difference between a rendered image and the ground truth image for the task is shown in Fig. 4.

### B. Robot experiments

To demonstrate the flexibility and efficiency of our method, we conduct several real-world experiments across both indoor and outdoor environments. We measure the ability of our framework to load, localize and then navigate to the target. Then, we demonstrate that our method can be applied to completely unknown maps and follow the utility signal to complete the task. The task completion oracle  $\psi$  uses a VLM with a prompt requesting yes or no to terminate the task. Example outputs from our experiments are shown in Fig. 3.

**Metrics.** We compute the path length  $PL$  of the trajectory taken by the robot in each experiment. We compare this against two other path lengths,  $SP$  and  $GT$ . After the experiment is complete and the map is available, we compute the shortest path  $SP$  on the full planning graph. This ablates away any odometry error since our traveled path and the planning graph are built on the same set of odometry measurements. To obtain the length of the optimal path  $GT$  from the starting position to the inferred goal in the outdoor experiments, we measure the path length from GPS coordinates annotated by a human on Google Earth. For indoor experiments, we measure the shortest path from the start to goal with a rangefinder. We measure the competitive ratio (listed *ratio* in Tab. V) of the distance measured by the visual odometry on our robot and these privileged distance measurements, given by  $\frac{SP}{PL}$  and  $\frac{GT}{PL}$  respectively. To show the scale of our experiments, we measure and report the approximate area of the operational area of the environment for each experiment from Google Earth, and the number of Gaussians in the map.

**Experiment Areas.** We conduct our experiments in an urban office complex (shown in Fig. 5) with office space, parking lots, and an outdoor park.

1) *Navigation in pre-built map:* To show how our sparse hierarchical map can be used for navigation, we conduct an experiment *Outdoor1* where the robot uses a pre-built map to identify and plan a path to a region of interest. An example is shown in Fig. 8. In this experiment, we first tele-operate the robot to a dock several hundred meters from the starting position and save the map. On a separate run, the map is loaded on the robot. The robot is given the task ‘navigate to entrance to pier’. The task relevancy is computed across the submaps and their regions, and the submap with the highest



**Fig. 3:** Qualitative results showing the output of the VLM when the task terminates.

Experiment	Task	Prior Map	Distance (m)				Area (m <sup>2</sup> )	Num. of Gaussians
			PL (m)	SP (m / ratio)	GT (m / ratio)			
Outdoor1	Navigate to entrance to pier	Yes	185.78	—	184.86	0.99	3346.5	2661562
Indoor1	Find cushions	No	72.53	34.87	0.48	29.72	0.41	973.28
Indoor2	Find plants, Exit building	No	44.55	31.60	0.71	30.16	0.68	973.28
Outdoor2	Inspect road blockage	No	94.25	45.16	0.48	43.52	0.46	1063.57
Outdoor3	Find parking lot	No	69.19	46.439	0.67	43.22	0.62	1280.10
Outdoor4	Find river near road	No	742.42	473.64	0.64	472.55	0.64	17791.14
Outdoor5	Find boardwalk near road	No	1257.53	688.90	0.55	671.76	0.53	21870.34
								11279776

**TABLE V:** Overview of robot experiments. *Prior* indicates that a prior *PL* refers to path length, *SP* refers to the shortest path computed on the full planning graph after the experiment is complete, and *GT* refers to the ground truth.

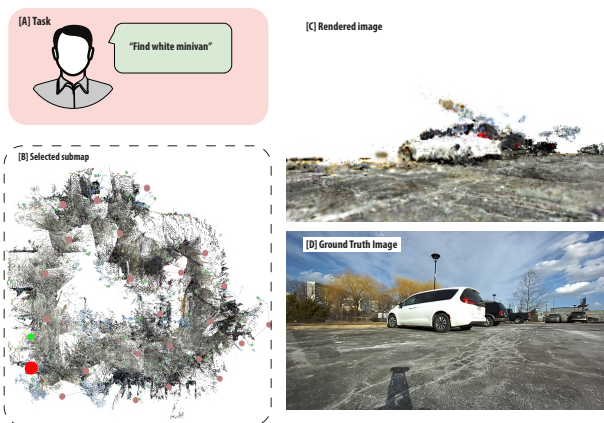


**Fig. 4:** [A] shows the task provided to our method. [B] shows the selected submap and region in the bottom-left with highest relevance. [C] shows the rendered image from the vantage point with the highest relevance to the task. [D] shows the ground truth image.

utility is identified. The robot plans a path to the submap of interest and navigates to the goal.



**Fig. 5:** The outdoor experiment areas for our experiments. Our park experiments are in the highlighted yellow areas. The parking lots are in red and blue.

**Results.** Our results for this experiment are reported in Table V. As expected, our method performs close to the ground truth since it also has access to the true map of the environment. The qualitative results of the VLM query for the termination of the task is shown in Fig. 6.



**Fig. 6:** The user-specified task and the description received on termination of the task. The VLM is queried when the relevancy of the language features obtained from the image exceeds a threshold.

2) *Navigation with no prior map*: We conduct six real-world experiments – two indoor and four outdoor. In these experiments, the robot starts off with no prior map or information of the environment. Given a user-specified task, the robot proceeds to incrementally build a metric-semantic map of the environment and uses relevant information in the map to complete the task.

**Indoor.** For *Indoor1*, we perform a simple object search of ‘find plants’ and then demonstrate re-tasking the robot to ‘exit the building’. In the second indoor experiment *Indoor2*, we show that our approach is able to leverage the semantic relationships between objects in the environment to complete tasks. With the task ‘find cushions’, the robot is able to identify chairs and couches as areas of high relevance to the task and proceeds to inspect them, eventually successfully locating the cushions. Visualizations of the experiment are provided in Fig. 7.

**Outdoor.** For our outdoor experiments, we consider the following:

- 1) In *Outdoor2*, we use an under-specified task ‘inspect road blockage’ and the robot leverages semantics of the pavement to search for and identify obstructions.
- 2) In *Outdoor3*, the robot is tasked with ‘find parking lot’ while starting close to the entrance of a building.
- 3) In *Outdoor4* and *Outdoor5*, we conduct large-scale experiments in the park. A visualization of task relevancy and the ground truth trajectory is shown in Fig. 8.

**Results.** We present an overview of the robot experiments in Table V. The competitive ratio of our method is  $\sim 0.59$  on



**Fig. 7:** Robot executing the task ‘find cushions’ starting at [A]. The robot incrementally constructs a map with language-embedded Gaussian splatting and identifies and navigates to regions in the map with high relevance. The VLM is queried at vantage points [B], [C], [D]. The images acquired at [B] and [C] have the second-order association of couches but no cushions. The task only terminates at [D] when the cushion is found.

*SP* and  $\sim 0.56$  on *GT*. This shows that our tasks require some exploration but in general, our method performs at least half as well as a privileged baseline. In our experiments, our method is also able to store over an order of a million Gaussians on-board the robot.

## VI. LIMITATIONS

One of the primary limitations of this method is its heavy dependence on the quality of the external odometry solution. While it is possible to incorporate loop closures into the process, the system is fundamentally reliant on the external module’s ability to accurately detect and handle these loop closures. Furthermore, the success of the method is dependent on the quality of the visual data—both the images and depth information—as well as the viewpoint from which they are captured. Poor-quality images, inaccurate depth mea-

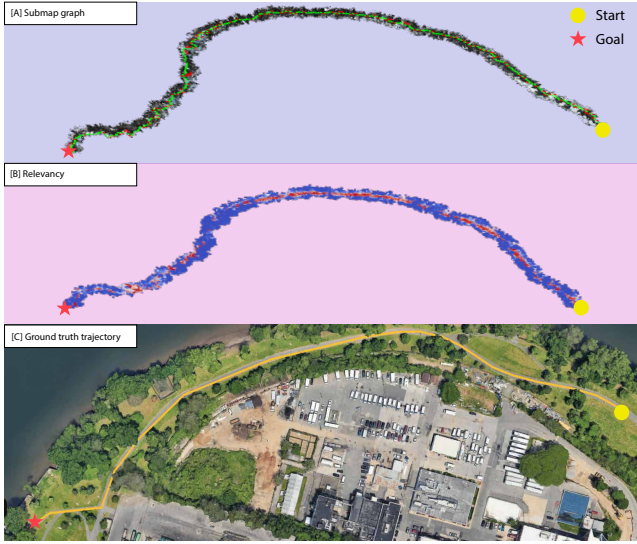


**Fig. 8:** [A] The map built from the task "Find boardwalk near road". The colored Gaussian points and the submap nodes (red and green circles) are visualized. The prior hierarchical graph can then be used to retrieve and navigate in the map. The shortest path (SP) to the boardwalk is shown with the green nodes. [B] The task relevancy of the Gaussians is colored blue (low) to red (high). [C] The ground truth trajectory (GT) is overlaid in yellow on an image from Google Earth to highlight the scale of the experiments.

surements, or suboptimal viewpoints can severely impact the system's ability to generate accurate task-driven semantics, as these factors form the core of the data used to interpret and solve tasks. Empirically, the compressed CLIP features retain sufficient information for the tasks we consider but may not work for more abstract tasks. We also do not consider the orientation of the robot at the discrete planning stage, which might result in the robot failing to complete the task by mapping only a portion of the object of interest. Lastly, the method faces challenges when dealing with very abstract tasks. While it performs well for tasks with concrete and well-defined semantics, it may struggle with tasks that require a deeper understanding or decomposition of more abstract concepts. In such cases, additional tools, such as large language models (LLMs), may be necessary to decompose the tasks into more manageable components, further complicating the overall process and potentially adding another layer of complexity.

## VII. CONCLUSION

In this paper, we develop a framework and methodology that allows robots to autonomously explore and navigate unstructured environments to accomplish tasks that are specified using natural language. Central to our approach is a hierarchical representation built on language-embedded Gaussian splatting that can be run on-board a robot in real time. We use indoor and outdoor experiments traversing hundreds of meters to show the robustness of our approach and our ability to build large-scale maps and identify semantically relevant objects in diverse environments. Our method does not rely on the

presence of structure or rich semantics in the scene and can be applied in general settings. In future work, we plan to deploy a distilled LLM on the robot for task decomposition to enable more abstract reasoning of tasks. While this paper empirically evaluates this method on largely 2D environments, in future work we will consider multi-floor buildings and large environments with elevation changes.

## REFERENCES

- [1] David Lattanzi and Gregory Miller. Review of robotic infrastructure inspection systems. *Journal of Infrastructure Systems*, 23(3):04017004, 2017.
- [2] Timothy H Chung, Viktor Orehov, and Angela Maio. Into the robotic depths: analysis and insights from the darpa subterranean challenge. *Annual Review of Control, Robotics, and Autonomous Systems*, 6(1):477–502, 2023.
- [3] Geert-Jan M Kruijff, Fiora Pirri, Mario Gianni, Panagiotis Papadakis, Matia Pizzoli, Arnab Sinha, Viatcheslav Tretyakov, Thorsten Linder, Emanuele Pianese, Salvatore Corrao, et al. Rescue robots at earthquake-hit mirandola, Italy: A field report. In *2012 IEEE international symposium on safety, security, and rescue robotics (SSRR)*, pages 1–8. IEEE, 2012.
- [4] Spyros Fountas, Nikos Mylonas, Ioannis Malounas, Efthymios Rodias, Christoph Hellmann Santos, and Erik Pekkeriet. Agricultural robotics for field operations. *Sensors*, 20(9):2672, 2020.
- [5] Bernhard Kerbl, Georgios Kopanas, Thomas Leimkühler, and George Drettakis. 3d gaussian splatting for real-time radiance field rendering. *ACM Transactions on Graphics*, 42(4):1–14, 2023.
- [6] Monika Wysoczańska, Oriane Siméoni, Michaël Ramamonjisoa, Andrei Bursuc, Tomasz Trzciński, and Patrick Pérez. Clip-dinoiser: Teaching clip a few dino tricks for open-vocabulary semantic segmentation. In *European Conference on Computer Vision*, pages 320–337. Springer, 2025.
- [7] Benjamin Charrow, Sikang Liu, Vijay Kumar, and Nathan Michael. Information-theoretic mapping using cauchy-schwarz quadratic mutual information. In *2015 IEEE International Conference on Robotics and Automation (ICRA)*, pages 4791–4798. IEEE, 2015.
- [8] Kelsey Saulnier, Nikolay Atanasov, George J Pappas, and Vijay Kumar. Information theoretic active exploration in signed distance fields. In *2020 IEEE International Conference on Robotics and Automation (ICRA)*, pages 4080–4085. IEEE, 2020.
- [9] Arash Asgharivaskasi and Nikolay Atanasov. Semantic octree mapping and shannon mutual information computation for robot exploration. *IEEE Transactions on Robotics*, 39(3):1910–1928, 2023.
- [10] Shi Bai, Jinkun Wang, Fanfei Chen, and Brendan Englot. Information-theoretic exploration with bayesian optimization. In *2016 IEEE/RSJ International Conference on Intelligent Robots and Systems (IROS)*, pages 1816–1822, 2016.

[11] Lukas Schmid, Michael Pantic, Raghav Khanna, Lionel Ott, Roland Siegwart, and Juan Nieto. An efficient sampling-based method for online informative path planning in unknown environments. *IEEE Robotics and Automation Letters*, 5(2):1500–1507, 2020.

[12] Andreas Bircher, Mina Kamel, Kostas Alexis, Helen Oleynikova, and Roland Siegwart. Receding horizon” next-best-view” planner for 3d exploration. In *2016 IEEE international conference on robotics and automation (ICRA)*, pages 1462–1468. IEEE, 2016.

[13] Christos Papachristos, Shehryar Khattak, and Kostas Alexis. Uncertainty-aware receding horizon exploration and mapping using aerial robots. In *2017 IEEE International Conference on Robotics and Automation (ICRA)*, pages 4568–4575, 2017.

[14] Mihir Dharmadhikari, Tung Dang, Lukas Solanka, Johannes Loje, Huan Nguyen, Nikhil Khedekar, and Kostas Alexis. Motion primitives-based path planning for fast and agile exploration using aerial robots. In *2020 IEEE International Conference on Robotics and Automation (ICRA)*, pages 179–185, 2020.

[15] Lukas Schmid, Victor Reijgwart, Lionel Ott, Juan Nieto, Roland Siegwart, and Cesar Cadena. A unified approach for autonomous volumetric exploration of large scale environments under severe odometry drift. *IEEE Robotics and Automation Letters*, 6(3):4504–4511, 2021.

[16] Yuezhan Tao, Yuwei Wu, Beiming Li, Fernando Cladera, Alex Zhou, Dinesh Thakur, and Vijay Kumar. SEER: Safe efficient exploration for aerial robots using learning to predict information gain. In *2023 IEEE International Conference on Robotics and Automation (ICRA)*, pages 1235–1241. IEEE, 2023.

[17] Yuezhan Tao, Xu Liu, Igor Spasojevic, Saurav Agarwal, and Vijay Kumar. 3d active metric-semantic slam. *IEEE Robotics and Automation Letters*, pages 1–8, 2024.

[18] Xuran Pan, Zihang Lai, Shiji Song, and Gao Huang. Activenerf: Learning where to see with uncertainty estimation. In *European Conference on Computer Vision*, pages 230–246. Springer, 2022.

[19] Soomin Lee, Le Chen, Jiahao Wang, Alexander Liniger, Suryansh Kumar, and Fisher Yu. Uncertainty guided policy for active robotic 3d reconstruction using neural radiance fields. *IEEE Robotics and Automation Letters*, 7(4):12070–12077, 2022.

[20] Huangying Zhan, Jiyang Zheng, Yi Xu, Ian Reid, and Hamid Rezatofighi. Activemap: Radiance field for active mapping and planning. *arXiv preprint arXiv:2211.12656*, 2022.

[21] Yunlong Ran, Jing Zeng, Shibo He, Jiming Chen, Lincheng Li, Yingfeng Chen, Gimhee Lee, and Qi Ye. Neurar: Neural uncertainty for autonomous 3d reconstruction with implicit neural representations. *IEEE Robotics and Automation Letters*, 8(2):1125–1132, 2023.

[22] Siming He, Christopher D Hsu, Dexter Ong, Yifei Simon Shao, and Pratik Chaudhari. Active perception using neural radiance fields. *arXiv preprint arXiv:2310.09892*, 2023.

[23] Siming He, Yuezhan Tao, Igor Spasojevic, Vijay Kumar, and Pratik Chaudhari. An active perception game for robust autonomous exploration, 2024.

[24] Zike Yan, Haoxiang Yang, and Hongbin Zha. Active neural mapping. In *Proceedings of the IEEE/CVF International Conference on Computer Vision*, pages 10981–10992, 2023.

[25] Ziyue Feng, Huangying Zhan, Zheng Chen, Qingan Yan, Xiangyu Xu, Changjiang Cai, Bing Li, Qilun Zhu, and Yi Xu. Naruto: Neural active reconstruction from uncertain target observations. In *Proceedings of the IEEE/CVF Conference on Computer Vision and Pattern Recognition*, pages 21572–21583, 2024.

[26] Wen Jiang, Boshu Lei, and Kostas Daniilidis. Fisherrf: Active view selection and uncertainty quantification for radiance fields using fisher information, 2023.

[27] Rui Jin, Yuman Gao, Yingjian Wang, Haojian Lu, and Fei Gao. Gs-planner: A gaussian-splatting-based planning framework for active high-fidelity reconstruction, 2024.

[28] Zijun Xu, Rui Jin, Ke Wu, Yi Zhao, Zhiwei Zhang, Jieru Zhao, Fei Gao, Zhongxue Gan, and Wenchao Ding. Hgs-planner: Hierarchical planning framework for active scene reconstruction using 3d gaussian splatting. *arXiv preprint arXiv:2409.17624*, 2024.

[29] Yuezhan Tao, Dexter Ong, Varun Murali, Igor Spasojevic, Pratik Chaudhari, and Vijay Kumar. Rt-guide: Real-time gaussian splatting for information-driven exploration. *arXiv preprint arXiv:2409.18122*, 2024.

[30] Nikhil Keetha, Jay Karhade, Krishna Murthy Jatavallabhula, Gengshan Yang, Sebastian Scherer, Deva Ramanan, and Jonathon Luiten. Splatam: Splat, track & map 3d gaussians for dense rgb-d slam. In *Proceedings of the IEEE/CVF Conference on Computer Vision and Pattern Recognition*, 2024.

[31] Hidenobu Matsuki, Riku Murai, Paul HJ Kelly, and Andrew J Davison. Gaussian splatting slam. In *Proceedings of the IEEE/CVF Conference on Computer Vision and Pattern Recognition*, pages 18039–18048, 2024.

[32] Zhixi Peng, Tianjia Shao, Yong Liu, Jingke Zhou, Yin Yang, Jingdong Wang, and Kun Zhou. Rtg-slam: Real-time 3d reconstruction at scale using gaussian splatting. In *ACM SIGGRAPH 2024 Conference Papers*, pages 1–11, 2024.

[33] Jiarui Hu, Xianhao Chen, Boyin Feng, Guanglin Li, Liangjing Yang, Hujun Bao, Guofeng Zhang, and Zhaopeng Cui. Cg-slam: Efficient dense rgb-d slam in a consistent uncertainty-aware 3d gaussian field. In *European Conference on Computer Vision*, pages 93–112. Springer, 2025.

[34] Timothy Chen, Ola Shorinwa, Weijia Zeng, Joseph Bruno, Philip Dames, and Mac Schwager. Splat-nav: Safe real-time robot navigation in gaussian splatting maps. *arXiv preprint arXiv:2403.02751*, 2024.

[35] Alec Radford, Jong Wook Kim, Chris Hallacy, Aditya Ramesh, Gabriel Goh, Sandhini Agarwal, Girish Sastry,

Amanda Askell, Pamela Mishkin, Jack Clark, et al. Learning transferable visual models from natural language supervision. In *International conference on machine learning*, pages 8748–8763. PMLR, 2021.

[36] Jin-Chuan Shi, Miao Wang, Hao-Bin Duan, and Shao-Hua Guan. Language embedded 3d gaussians for open-vocabulary scene understanding. In *Proceedings of the IEEE/CVF Conference on Computer Vision and Pattern Recognition*, pages 5333–5343, 2024.

[37] Minghan Qin, Wanhua Li, Jiawei Zhou, Haoqian Wang, and Hanspeter Pfister. Langsplat: 3d language gaussian splatting. In *Proceedings of the IEEE/CVF Conference on Computer Vision and Pattern Recognition*, pages 20051–20060, 2024.

[38] Guibiao Liao, Jiankun Li, Zhenyu Bao, Xiaoqing Ye, Jingdong Wang, Qing Li, and Kanglin Liu. Clip-gs: Clip-informed gaussian splatting for real-time and view-consistent 3d semantic understanding. *arXiv preprint arXiv:2404.14249*, 2024.

[39] Justin Yu, Kush Hari, Kishore Srinivas, Karim El-Refai, Adam Rashid, Chung Min Kim, Justin Kerr, Richard Cheng, Muhammad Zubair Irshad, Ashwin Balakrishna, et al. Language-embedded gaussian splats (legs): Incrementally building room-scale representations with a mobile robot. In *2024 IEEE/RSJ International Conference on Intelligent Robots and Systems (IROS)*, pages 13326–13332. IEEE, 2024.

[40] Xingxing Zuo, Pouya Samangouei, Yunwen Zhou, Yan Di, and Mingyang Li. Fmgs: Foundation model embedded 3d gaussian splatting for holistic 3d scene understanding. *International Journal of Computer Vision*, pages 1–17, 2024.

[41] Justin Kerr, Chung Min Kim, Ken Goldberg, Angjoo Kanazawa, and Matthew Tancik. Lerf: Language embedded radiance fields. In *Proceedings of the IEEE/CVF International Conference on Computer Vision*, pages 19729–19739, 2023.

[42] Liyuan Zhu, Yue Li, Erik Sandström, Shengyu Huang, Konrad Schindler, and Iro Armeni. Loopsplat: Loop closure by registering 3d gaussian splats. *arXiv preprint arXiv:2408.10154*, 2024.

[43] Vladimir Yugay, Yue Li, Theo Gevers, and Martin R Oswald. Gaussian-slam: Photo-realistic dense slam with gaussian splatting. *arXiv preprint arXiv:2312.10070*, 2023.

[44] Tung Dang, Christos Papachristos, and Kostas Alexis. Autonomous exploration and simultaneous object search using aerial robots. In *2018 IEEE Aerospace Conference*, pages 1–7. IEEE, 2018.

[45] Xu Liu, Jiuzhou Lei, Ankit Prabhu, Yuezhan Tao, Igor Spasojevic, Pratik Chaudhari, Nikolay Atanasov, and Vijay Kumar. Slideslam: Sparse, lightweight, decentralized metric-semantic slam for multi-robot navigation. *arXiv preprint arXiv:2406.17249*, 2024.

[46] Iro Armeni, Zhi-Yang He, JunYoung Gwak, Amir R Zamir, Martin Fischer, Jitendra Malik, and Silvio Savarese. 3d scene graph: A structure for unified semantics, 3d space, and camera. In *IEEE/CVF Int. Conf. on Computer Vision*, pages 5664–5673, 2019.

[47] Shun-Cheng Wu, Johanna Wald, Keisuke Tateno, Nassir Navab, and Federico Tombari. Scenegraphfusion: Incremental 3d scene graph prediction from rgb-d sequences. In *Proc. of IEEE Conf. on Computer Vision and Pattern Recognition*, pages 7515–7525, 2021.

[48] Samuel Looper, Javier Rodriguez-Puigvert, Roland Siegwart, Cesar Cadena, and Lukas Schmid. 3d vsg: Long-term semantic scene change prediction through 3d variable scene graphs. In *IEEE Int. Conf. on Robotics & Automation*, pages 8179–8186. IEEE, 2023.

[49] Nathan Hughes, Yun Chang, Siyi Hu, Rajat Talak, Rumaia Abdulhai, Jared Strader, and Luca Carlone. Foundations of spatial perception for robotics: Hierarchical representations and real-time systems. *The International Journal of Robotics Research*, 2024.

[50] Hriday Bavle, Jose Luis Sanchez-Lopez, Muhammad Shaheer, Javier Civera, and Holger Voos. S-graphs+: Real-time localization and mapping leveraging hierarchical representations. *IEEE Robotics and Automation Letters*, 8(8):4927–4934, 2023.

[51] Jared Strader, Nathan Hughes, William Chen, Alberto Speranzon, and Luca Carlone. Indoor and outdoor 3d scene graph generation via language-enabled spatial ontologies. *IEEE Robotics and Automation Letters*, 9(6):4886–4893, 2024.

[52] Dominic Maggio, Yun Chang, Nathan Hughes, Matthew Trang, Dan Griffith, Carlyn Dougherty, Eric Cristofalo, Lukas Schmid, and Luca Carlone. Clio: Real-time task-driven open-set 3d scene graphs. *arXiv preprint arXiv:2404.13696*, 2024.

[53] Venkata Naren Devarakonda, Raktim Gautam Goswami, Ali Umut Kaypak, Naman Patel, Rooholla Khorrambakht, Prashanth Krishnamurthy, and Farshad Khorrami. Orionnav: Online planning for robot autonomy with context-aware llm and open-vocabulary semantic scene graphs. *arXiv preprint arXiv:2410.06239*, 2024.

[54] Qiao Gu, Alihusein Kuwajerwala, Sacha Morin, Krishna Murthy Jatavallabhula, Bipasha Sen, Aditya Agarwal, Corban Rivera, William Paul, Kirsty Ellis, Rama Chellappa, Chuang Gan, Celso Miguel de Melo, Joshua B. Tenenbaum, Antonio Torralba, Florian Shkurti, and Liam Paull. Conceptgraphs: Open-vocabulary 3d scene graphs for perception and planning. *International Conference on Robotics and Automation*, 2024.

[55] Abdelrhman Werby, Chenguang Huang, Martin Büchner, Abhinav Valada, and Wolfram Burgard. Hierarchical open-vocabulary 3d scene graphs for language-grounded robot navigation. In *First Workshop on Vision-Language Models for Navigation and Manipulation at ICRA 2024*, 2024.

[56] Sotiris Papatheodorou, Nils Funk, Dimos Tzoumanikas, Christopher Choi, Binbin Xu, and Stefan Leutenegger. Finding things in the unknown: Semantic object-centric

exploration with an mav. In *2023 IEEE International Conference on Robotics and Automation (ICRA)*, pages 3339–3345. IEEE, 2023.

[57] Georgios Georgakis, Bernadette Bucher, Karl Schmeck-peper, Siddharth Singh, and Kostas Daniilidis. Learning to map for active semantic goal navigation. *arXiv preprint arXiv:2106.15648*, 2021.

[58] Zhirui Dai, Arash Asgharivaskasi, Thai Duong, Shusen Lin, Maria-Elizabeth Tzes, George Pappas, and Nikolay Atanasov. Optimal scene graph planning with large language model guidance, 2024.

[59] Saeid Amiri, Kishan Chandan, and Shiqi Zhang. Reasoning with scene graphs for robot planning under partial observability. *IEEE Robotics and Automation Letters*, 7(2):5560–5567, 2022.

[60] Zachary Ravichandran, Lisa Peng, Nathan Hughes, J Daniel Griffith, and Luca Carlone. Hierarchical representations and explicit memory: Learning effective navigation policies on 3d scene graphs using graph neural networks. In *2022 International Conference on Robotics and Automation (ICRA)*, pages 9272–9279. IEEE, 2022.

[61] Naoki Yokoyama, Sehoon Ha, Dhruv Batra, Jiuguang Wang, and Bernadette Bucher. Vlfm: Vision-language frontier maps for zero-shot semantic navigation. In *2024 IEEE International Conference on Robotics and Automation (ICRA)*, pages 42–48. IEEE, 2024.

[62] Zachary Ravichandran, Varun Murali, Mariliza Tzes, George J Pappas, and Vijay Kumar. Spine: Online semantic planning for missions with incomplete natural language specifications in unstructured environments. *arXiv preprint arXiv:2410.03035*, 2024.

[63] Xiaoyi Dong, Jianmin Bao, Yinglin Zheng, Ting Zhang, Dongdong Chen, Hao Yang, Ming Zeng, Weiming Zhang, Lu Yuan, Dong Chen, et al. Maskclip: Masked self-distillation advances contrastive language-image pre-training. In *Proceedings of the IEEE/CVF Conference on Computer Vision and Pattern Recognition*, pages 10995–11005, 2023.

[64] Maxime Oquab, Timothée Darcet, Théo Moutakanni, Huy Vo, Marc Szafraniec, Vasil Khalidov, Pierre Fernandez, Daniel Haziza, Francisco Massa, Alaaeldin El-Nouby, et al. Dinov2: Learning robust visual features without supervision. *arXiv preprint arXiv:2304.07193*, 2023.

[65] David A Ross, Jongwoo Lim, Ruei-Sung Lin, and Ming-Hsuan Yang. Incremental learning for robust visual tracking. *International journal of computer vision*, 77:125–141, 2008.

[66] Tsung-Yi Lin, Michael Maire, Serge Belongie, James Hays, Pietro Perona, Deva Ramanan, Piotr Dollár, and C Lawrence Zitnick. Microsoft coco: Common objects in context. In *Computer Vision–ECCV 2014: 13th European Conference, Zurich, Switzerland, September 6–12, 2014, Proceedings, Part V 13*, pages 740–755. Springer, 2014.

[67] Sikang Liu, Nikolay Atanasov, Kartik Mohta, and Vijay Kumar. Search-based motion planning for quadrotors using linear quadratic minimum time control. In *2017 IEEE/RSJ international conference on intelligent robots and systems (IROS)*, pages 2872–2879. IEEE, 2017.

[68] Bo Li, Yuanhan Zhang, Dong Guo, Renrui Zhang, Feng Li, Hao Zhang, Kaichen Zhang, Peiyuan Zhang, Yanwei Li, Ziwei Liu, et al. Llava-onevision: Easy visual task transfer. *arXiv preprint arXiv:2408.03326*, 2024.

[69] Angela Dai, Angel X. Chang, Manolis Savva, Maciej Halber, Thomas Funkhouser, and Matthias Nießner. Scannet: Richly-annotated 3d reconstructions of indoor scenes. In *Proc. Computer Vision and Pattern Recognition (CVPR), IEEE*, 2017.

[70] Krishna Murthy Jatavallabhula, Alihusein Kuwajerwala, Qiao Gu, Mohd Omama, Tao Chen, Alaa Maalouf, Shuang Li, Ganesh Iyer, Soroush Saryazdi, Nikhil Keetha, et al. Conceptfusion: Open-set multimodal 3d mapping. *arXiv preprint arXiv:2302.07241*, 2023.

[71] Chunge Bai, Tao Xiao, Yajie Chen, Haoqian Wang, Fang Zhang, and Xiang Gao. Faster-lio: Lightweight tightly coupled lidar-inertial odometry using parallel sparse incremental voxels. *IEEE Robotics and Automation Letters*, 7(2):4861–4868, 2022.

[72] Z. Wang, E.P. Simoncelli, and A.C. Bovik. Multiscale structural similarity for image quality assessment. In *The Thirty-Seventh Asilomar Conference on Signals, Systems & Computers, 2003*, volume 2, pages 1398–1402 Vol.2, 2003.

[73] Richard Zhang, Phillip Isola, Alexei A Efros, Eli Shechtman, and Oliver Wang. The unreasonable effectiveness of deep features as a perceptual metric. In *CVPR*, 2018.

[74] Karmesh Yadav, Ram Ramrakhyta, Santhosh Kumar Ramakrishnan, Theo Gervet, John Turner, Aaron Gokaslan, Noah Maestre, Angel Xuan Chang, Dhruv Batra, Manolis Savva, et al. Habitat-matterport 3d semantics dataset. In *Proceedings of the IEEE/CVF Conference on Computer Vision and Pattern Recognition*, pages 4927–4936, 2023.